Bitlis Eren Üniversitesi Fen Bilimleri Dergisi
BİTLİS EREN UNIVERSITY JOURNAL OF SCIENCE
ISSN: 2147-3129/e-ISSN: 2147-3188
VOLUME: 13 NO: 4 PAGE: 1314-1324 YEAR: 2024
DOI: 10.17798/bitlisfen.1558208

Exploring Radiation Shielding Properties of Lanthanide Elements

Nuray YAVUZKANAT[1*]

[1]*Bitlis Eren University, Faculty of Art and Sciences, Physics Department, Bitlis, Türkiye (ORCID: 0000-0001-5055-9185)*

Keywords: Lanthanides, LAC, HVL, EABF, EBF, GATE.

Abstract

In this work, the radiation shielding properties of Lanthanide elements were studied using the EpiXS program and GATE simulation, which agreed well with each other, based on some key parameters such as MAC, LAC, HVL, MFP, EABF, and EBF. It was observed that at lower energies of gamma-rays, the values of MAC and LAC are maximum, which decrease with the increase in energy due to reduced photoelectric interactions. Photoelectric absorption edges couple with peaks in attenuation values; peaks for elements of the lower atomic number, La, Ce, Pr, and Nd, appear as two while the peaks for elements of higher atomic number are three due to the additional absorptions by L-shell sub- levels or M-shell. These peaks take place when the energy of photons meets the energy level of electron binding. While Lutetium has the highest and Europium has the lowest LAC values, Lutetium also has the lowest HVL and MFP values; thus, it has the best radiation shielding properties. The EABF and EBF reach their maximum in the medium energy range and then decrease. Lutetium has the lowest photon buildup, and Lanthanum has the highest EABF and EBF values for all the studied elements at all penetration depths.

1. Introduction

The Rare earth elements (REEs) consist of a total of 17 elements, which include scandium, yttrium, and the lanthanides, which are crucial for digital and low-emission technologies [1]. Although they are called rare earth elements (REEs), they are actually quite abundant in the crust of the Earth, with light REEs being as abundant as copper [1]. Most REE mines are found in carbonatite-related deposits, with China dominating their production and controlling much of their extraction, which is why they are considered critical raw materials [1], [2]. REEs are utilized in advanced consumer electronics, eco-friendly products, industrial and medical equipment, as well as in the defense systems [2]. Their high reactivity posed difficulties in refining them into pure metals, and effective separation techniques were not developed until the 20th century because of their chemical similarities [3].

REEs are extensively utilized in radiation protection because they can be easily molded and enhance the physical and chemical properties of materials [4], [5]. With the growing emphasis on nuclear energy over traditional fossil fuels, the role of shielding materials has become more prominent. This is especially true in industries such as non-destructive testing and radiotherapy, where effective shielding in high-energy environments is crucial [6], [7]. In their study, Jing and colleagues investigated the shielding properties of REEs composite materials. The results showed that REEs effectively absorb thermal neutrons and gamma rays, while also improving the mechanical properties of the protective composites [11].

Lanthanides, occupying atomic numbers 57 to 71 on the periodic table, are categorized into light (57-64) and heavy (65-71) REEs based on their electron configurations [8]. This group of elements, including the lanthanides from Lanthanum (La) to Lutetium (Lu), plays a crucial role in digital and low-carbon technologies because of their distinctive magnetic and luminescent characteristics, making them essential in industries such as magnets,

[1]Corresponding author: nyavuzkanat@beu.edu.tr

Received: 30.09.2024, Accepted: 02.12.2024

hydrogen alloys, catalysts, and electronics, with growing demand driven by advanced technologies [1], [8].

An understanding of the different phenomena arising due to interaction of radiation with matter provides insight into the manner by which the radiation is transmitted or penetrated through a medium. This knowledge aids in selecting appropriate shielding materials based on the type of radiation [9,10]. Radiation shielding materials traditionally include lead, iron, and tungsten. While these materials can provide as an effective shield against gamma rays, they are less successful in shielding against neutrons. Besides, they have a number of limitations, such as opacity to visible light, and there are problems related to lead's toxicity, weight, and lack of flexibility [11]-[14]. In their work, Jing et al. studied the shielding features of REEs composite materials. The results indicated that REEs were effective in absorbing thermal neutrons and gamma rays; they also contribute to the mechanical properties of the protective composites [11]. In another study, Cui et al. evaluated the shielding properties of some rare earth/polypropylene materials at a tube voltage of 120 kV. The study found that increasing the rare earth filler content was more effective in enhancing the composite's shielding performance than merely increasing its thickness [5].

Incorporating lanthanides, such as Eu_2O_3, increases the photon interaction and linear attenuation coefficient (LAC), enhancing radiation shielding capacity [24]. The lead borate glasses with high concentrations of Pb are excellent glass materials that provide good radiation shielding characteristics; however, they present some problems in relation to transparency because of certain radiation-induced changes in glass [25]. Incorporating rare earth elements, such as cerium and dysprosium oxides, can improve both the transparency and radiation shielding effectiveness of these glasses [25].

In this investigation, the characteristics associated with radiation shielding of lanthanides, were investigated using the EpiXS program [26] and Monte Carlo simulations performed with the GATE framework. The radiation shielding capability of the material depends on a parameter known as the mass attenuation coefficient (MAC) (μ/ρ). Further, the shielding properties such as linear attenuation coefficient (LAC), half-value layer (HVL), mean free path (MFP), energy absorption buildup factor (EABF), and exposure buildup factor (EBF) have been studied using this parameter. The results obtained from both EpiXS and GATE simulation offer an in-depth insight into the shielding capabilities of the lanthanide elements.

2. Material and Method

Table 1 presents the key properties of the studied Lanthanide elements, ranging from Lanthanum to Lutetium, including density (g/cm^3) [27], effective atomic number, and electron density. These parameters are crucial for evaluating the shielding effectiveness of each element, as they directly influence photon interaction and attenuation capabilities.

Table 1. Key properties of Lanthanide elements relevant to radiation shielding effectiveness.

Elements	Density* (g/cm^3)	Effective Atomic Number	Electron Density
Lanthanum (La)	6.15	57	2.4712
Cerium (Ce)	6.77	58	2.4928
Praseodymium (Pr)	6.77	59	2.5216
Neodymium (Nd)	7.01	60	2.5050
Promethium (Pm)	7.26	61	2.5335
Samarium (Sm)	7.52	62	2.4831
Europium (Eu)	5.24	63	2.4966
Gadolinium (Gd)	7.90	64	2.4509
Terbium (Tb)	8.23	65	2.4630
Dysprosium (Dy)	8.55	66	2.4459
Holmium (Ho)	8.80	67	2.4464
Erbium (Er)	9.07	68	2.4483
Thulium (Tm)	9.32	69	2.4597
Ytterbium (Yb)	6.90	70	2.4359
Lutetium (Lu)	9.84	71	2.4437

*Density values are sourced from PubChem's Periodic Table database [27].

The intensity I of a photon beam passing through a material with a thickness of *x* (in cm) is determined using the Beer-Lambert law, which is expressed by the equation:

$$I = I_0\, e^{-\mu x} \tag{1}$$

where μ (cm^{-1}) represents the LAC, encompassing all interactions such as coherent scattering, Compton scattering, and the photoelectric effect. The MAC, denoted μ_m (cm^2/g), quantifies the amount of radiation absorbed by a material and is given by:

$$\mu_m = \frac{\mu}{\rho} = \sum w_i \left(\frac{\mu_i}{\rho_i}\right) \tag{2}$$

where ρ (g/cm^3) is the material's density, and w_i indicates the weight fraction of the i^{th} element. The MFP is defined as the average distance a photon travels before undergoing an interaction and is related to the HVL, which is the thickness of material required to reduce the radiation intensity by half. The HVL and MFP can be calculated as follows:

$$HVL = \frac{ln\,2}{\mu}\ ,\ MFP = \frac{1}{\mu} \tag{3}$$

In this study, MFP refers to the mean free path, representing the average distance a photon travels in a material before interaction. On the other hand, mfp denotes a multiple of the mean free path, used to express relative penetration depths, such as '40 mfp' indicating 40 times the mean free path. The buildup factor quantifies the ratio of the total photon flux at a given point to the photon flux that reaches that point without interacting. This factor is divided into two categories: the EABF and the EBF. EABF quantifies the energy absorbed by the material during radiation interaction, whereas EBF refers to the energy absorbed or retained in the air [28], [29]. The buildup factor is incorporated into the photon intensity equation:

$$I\,(x) = B\, I_o\, e^{-\mu\, x} \tag{4}$$

where B represents the buildup parameter. This parameter can be equal to or greater than 1. In cases where the interacting material has a low thickness and the photon is mono-energetic, the B value is 1. In other cases, the buildup value becomes greater than 1 [30], [31].

The Energy Absorption Buildup Factor (EABF) and Exposure Buildup Factor (EBF) are calculated using Harima's geometric-progression (G-P) fitting formula, which is widely applied to various materials [32]. This formula uses specific G-P fitting coefficients, denoted as a, b, c, d, and X_k, which are determined for each material and photon energy level according to the following expression.

$$P = \frac{P_1(log\ Z_2 - log\ Z_{eq}) + P_2(log\ Z_{eq} - log\ Z_1)}{log\ Z_2 - log\ Z_1} \tag{5}$$

The P values represent the G-P fitting coefficients that correspond to the atomic numbers Z at the specified energy level. Z_{eq} is the effective atomic number, which is used to characterize the material's overall response to photon interactions based on its atomic composition at that energy. The buildup factor is defined in terms of the mfp using the G-P fitting parameters, as expressed in the following equations:

$$B(E,x) = 1 + (b-1)X \begin{cases} \frac{K^x - 1}{K-1} & K \neq 1 \\ x & K = 1 \end{cases} \tag{6}$$

$$K(E,x) = c\,x^a + d\,\frac{tanh\left(\frac{x}{X_k} - 2 - -tanh(-2)\right)}{1 - tanh(-2)} \tag{7}$$

$$for\ x \leq 40 mfp$$

E represents the photon energy and *x* is the mfp value. The coefficient b is associated with the buildup factor at 1 mfp. The parameter K(E,x) indicates the photon dose multiplier and accounts for the alteration in the spectrum's shape at 1 mfp [32].

In this study, a comparison was made between the values obtained using two different methods: the EpiXS software program and the Monte Carlo simulations performed with the GATE framework. The EpiXS software program is an open-access tool designed for users in the field. It incorporates EPICS2017, which is the photon and electron library derived from ENDF/B-VIII. In contrast, EPDL97 is the photon library based on ENDF/B-VI.8. EPICS2017 features updated binding energies and cross sections and has been linearized to facilitate Lin-Lin interpolation, enhancing the data resolution within the photon library. This linearization has significantly increased the data density in the photon library, whereas the data density in the electron library remained unchanged [26].

The Monte Carlo simulation method is used across a wide range of fields, from medical

physics to particle physics. Among the most well-known Monte Carlo codes is Geant4, along with other specialized codes such as PENELOPE, FLUKA, MCNP, and GATE, which are tailored to specific application areas [33]. Geant4 is a software written in C++ that simulates interactions of particles with matter. GATE, on the other hand, is an interface program that runs Geant4 simulations and is continuously updated through international collaborations, with its development being closely tied to updates in Geant4 itself [33].

The GATE modeling used in this study is based on the detailed descriptions provided in the works of T. Şahmaran and Yavuzkanat, as shown in Figure 1 [28]. The NaI(Tl) scintillation detector (2-inch diameter x 2-inch height), modeled as a cylindrical structure with a thin MgO reflector to enhance light collection, was equipped with an aluminum shield for radiation protection. To evaluate the gamma shielding effectiveness, the investigated shielding material was placed between the detector and the lead block. Measurements labeled as I_0 represent open-field conditions, taken without shielding, while the values recorded as I were obtained after radiation passed through the shielding material. The exponential relationship between I and I_0 allows for the calculation of the attenuation coefficient of the material, as given by Equation 1.

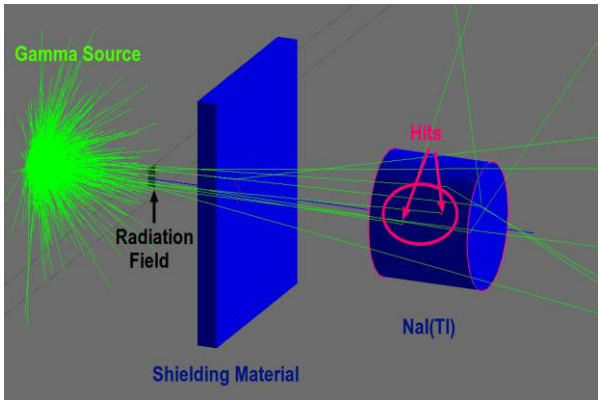

Figure 1. Configuration of the simulation setup, where gamma radiation is emitted isotropically from behind the blocks. The radiation field was arranged to be 1x1 cm² [28].

The percentage difference (PD) between the values was calculated using the formula:

$$PD = \left| \frac{LAC_{EpiXS} - LAC_{GATE}}{LAC_{EpiXS}} \right| x\ 100 \quad (8)$$

3. Results and Discussion

In Figures 2, as photon energy increases, the MAC and LAC for Lanthanide elements decrease. This trend indicates a decline in the likelihood of photoelectric interactions, as the energy becomes too high for photons to efficiently eject inner-shell electrons. Instead, Compton scattering and pair production processes become more significant, which are less energy-dependent. At very high photon energies, the MAC and LAC values stabilize, showing minimal variation. This stabilization occurs because the dominant attenuation mechanisms, such as Compton scattering and pair production, lead to a more constant attenuation behavior regardless of further increases in photon energy.

The MAC, LAC, HVL, and MFP for gamma energies ranging from 0.001 to 1000 MeV were determined using the EpiXS program for the Lanthanide group of elements. The results showed that these values were highest at low gamma ray energies and gradually decreased as the energy increased.

At lower photon energies (typically below 0.1 MeV or 100 keV), the sharp peaks are most likely due to photoelectric absorption edges, where the photon energy matches electrons' binding energy in the atom's inner shells. In Lanthanide group elements, the number of observed peaks (2 or 3) is related to their atomic structure. Elements with lower atomic numbers (La, Ce, Pr, and Nd) typically exhibit 2 peaks, corresponding to photon absorption in the K and L shells as observed in Figure 1. In contrast, elements with higher atomic numbers show 3 peaks due to additional absorption from the L-shell sub-levels (L1, L2, L3) or M-shell. The peaks occur when photon energy matches the binding energy of these electron shells, and as atomic number increases, more complex interactions lead to additional absorption edges and peaks.

As photon energy increases past these absorption edges, the effect of photoelectric absorption diminishes, leading to a gradual decline in both the MAC and LAC. This decrease is expected because the photoelectric absorption cross-section is inversely related to photon energy. At higher photon energies, beyond approximately 1 MeV, attenuation levels off as Compton scattering becomes the dominant interaction mechanism, with pair production also contributing at even higher energies. It was determined in Figures 2 (b) that Lutetium and Europium have the highest and lowest LAC values, respectively. In

Figure 2 (a), Lutetium and Lanthanum were found to have the highest and lowest MAC values, respectively.

According to Nagaraj et al. materials like Lanthanum polymer, Cerium polymer, Praseodymium polymer, Gadolinium texaphyrin polymer, Terbium co-ordination polymer and Erbium phosphate hydrate polymer were used to investigate X-ray/gamma, neutron, and EMI (electromagnetic interference) shielding properties [34]. Among them, Erbium phosphate hydrate showed the highest values in key shielding parameters such as mass attenuation coefficient (MAC) and effective atomic number (Z_{eff}). These findings suggest that Erbium phosphate hydrate polymer may be an ideal material for shielding against X-ray/gamma, neutron, and EMI radiation [34]. In our study, similar to this work, the MAC values are ranked from largest to smallest as follows: La < Ce < Pr < Gd < Tb < Er. Additionally, in our study examining all lanthanide group elements, the best results were observed in the order of Lutetium, Ytterbium, Thulium, and Erbium.

Figures 3 illustrate the variation in HVL and MFP values across the energy range of 0.001 to 1000 MeV. According to these figures, Lutetium exhibits the lowest HVL and MFP values as photon energy increases, indicating that it provides the most effective shielding capabilities among the Lanthanide elements. In contrast, Europium has the highest HVL and MFP values, reflecting its relatively lower shielding effectiveness. Lower HVL and MFP values generally signify better shielding capability, as these materials are more efficient at attenuating photon penetration. The observed differences in HVL and MFP values between Lutetium and Lanthanum can be attributed to their atomic numbers. Lutetium, with a higher atomic number (Z=71), has a denser electron cloud, which increases the likelihood of photon interactions, such as photoelectric absorption and Compton scattering. Consequently, this results in lower HVL and MFP values, reflecting a higher capacity for photon attenuation compared to Lanthanum (Z=57).

The differences between the Energy Absorption Buildup Factor (EABF) and the Exposure Buildup Factor (EBF) are primarily due to how each factor accounts for photon interactions in the material. EABF values are typically higher than EBF values because they consider not only the primary photon interactions but also cumulative effects from secondary photons produced through scattering processes. This cumulative interaction is especially noticeable in elements with higher atomic numbers (Z), where the increased electron density leads to enhanced photoelectric absorption and Compton scattering.

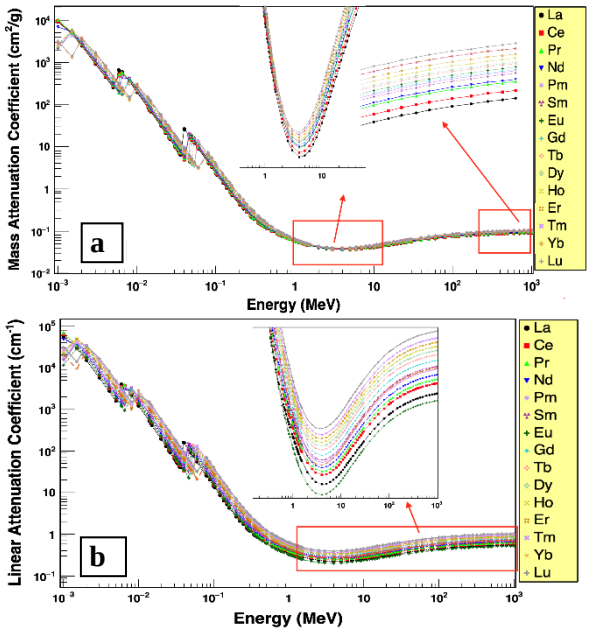

Figure 2. (a) MAC and **(b)** LAC values for Lanthanide group elements in the energy range of 0.001 to 1000 MeV.

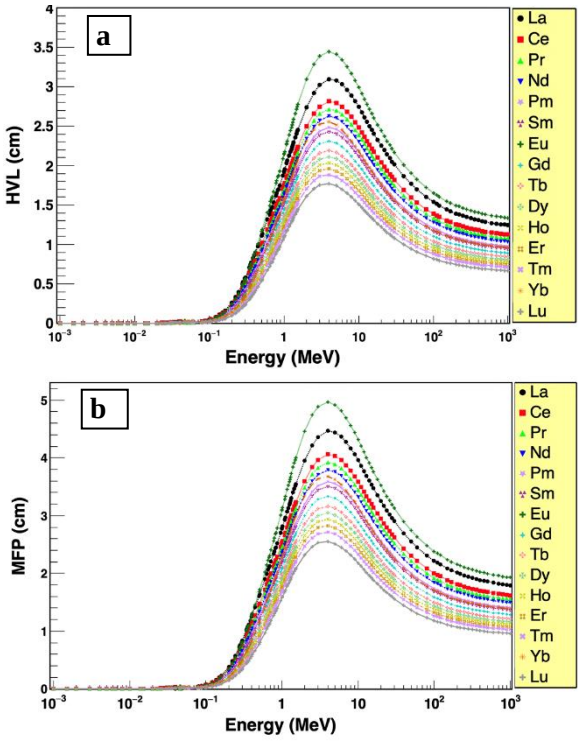

Figure 3. (a) HVL and **(b)** MFP values for Lanthanide group elements across the energy range of 0.001 to 1000 MeV.

Consequently, materials with higher Z values tend to exhibit higher EABF values, as their atomic structure promotes more significant photon attenuation and secondary photon production. In contrast, EBF values do not fully account for these secondary interactions, resulting in lower buildup values in comparison. This distinction highlights the role of atomic structure in influencing buildup factors, particularly as photon energy increases.

In Figure 4 and 5, the variation of the EABF and EBF for Lanthanide elements as a function of photon energy at various penetration depths (1, 10, 20, and 40 mfp). The graphs reveal that both EABF and EBF values initially increase, reaching a peak within the intermediate energy range, and then decrease as photon energy continues to rise. In the regions of low and high energy, the interactions responsible for the complete absorption of photons are photoelectric effects and pair production. As a result, photons have a shorter lifetime in the material. In contrast, Compton scattering predominates in the medium energy range, causing photons to stay in the material longer and resulting in higher EABF and EBF values. As shown in Figure 4 and 5, Lutetium exhibits the lowest photon buildup across all penetration depths, while Lanthanum shows the highest EABF and EBF values. This is because photons experience more scattering in Lanthanum, leading to greater photon buildup. As the photon path length through the material increases, or as the material thickness grows, scattering also increases, further raising the EABF and EBF values.

During the pair production process, the cross-section is proportional to Z^2, causing most photons to disappear, as in the photoelectric effect. Therefore, the EABF and EBF values are smaller in these energy regions. Photon energies above 1.02 MeV (the threshold for pair production) allow the pair production process to occur, with its interaction cross-section increasing in proportion to the square of the atomic number (Z^2). However, Compton scattering remains a significant competing process in this energy range, affecting photon interactions alongside pair production. Although pair production contributes to photon attenuation, its influence on the energy absorption buildup factor (EABF) and exposure buildup factor (EBF) is limited due to the concurrent impact of Compton scattering.

As a result, there is a less pronounced reduction in these factors, even in the energy range where pair production becomes more prominent. This is particularly evident in the graph (Figure 3), where no clear decrease in EABF values is observed above 1.2 MeV, despite pair production starting to take effect. This can be attributed to the ongoing significant contribution of Compton scattering at these higher energies, which offsets the potential reduction in EABF that might be expected solely from pair production.

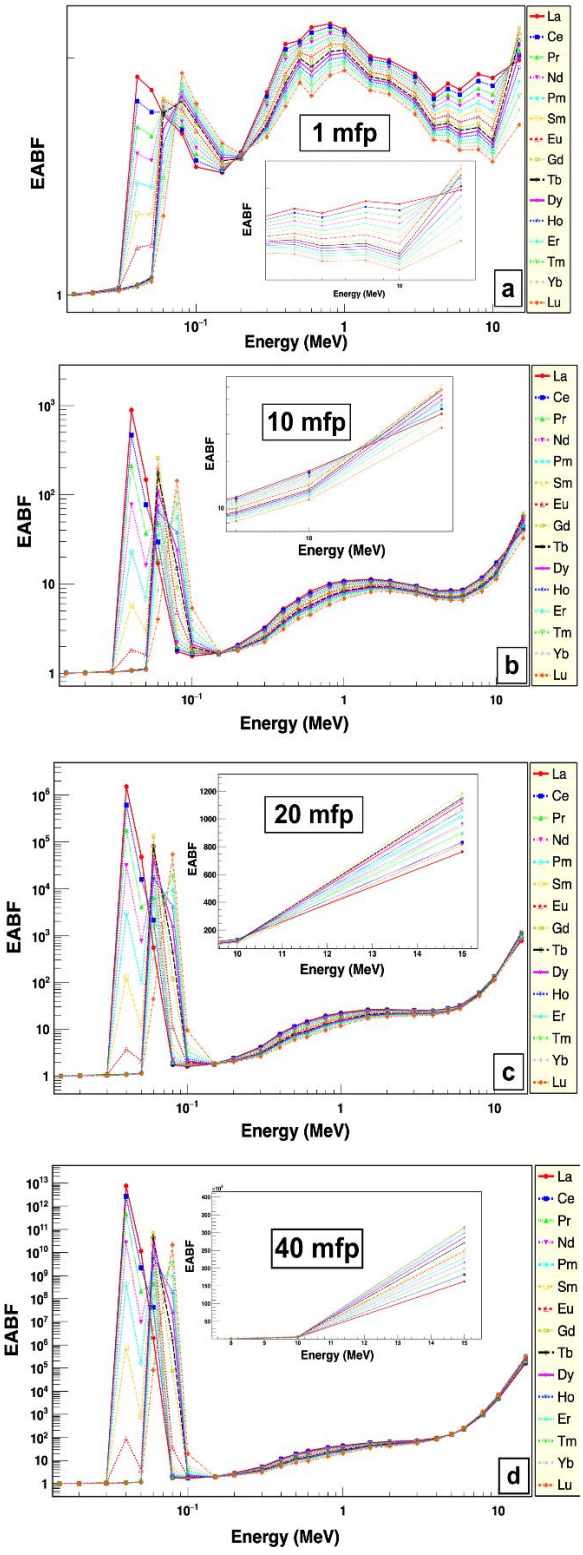

Figure 4. Variation of EABF with photon energy in the range of 0.015 to 15 MeV for Lanthanide group elements at various penetration depths for **(a)**1 mfp, **(b)** 10 mfp, **(c)** 20 mfp, **(d)** 40 mfp.

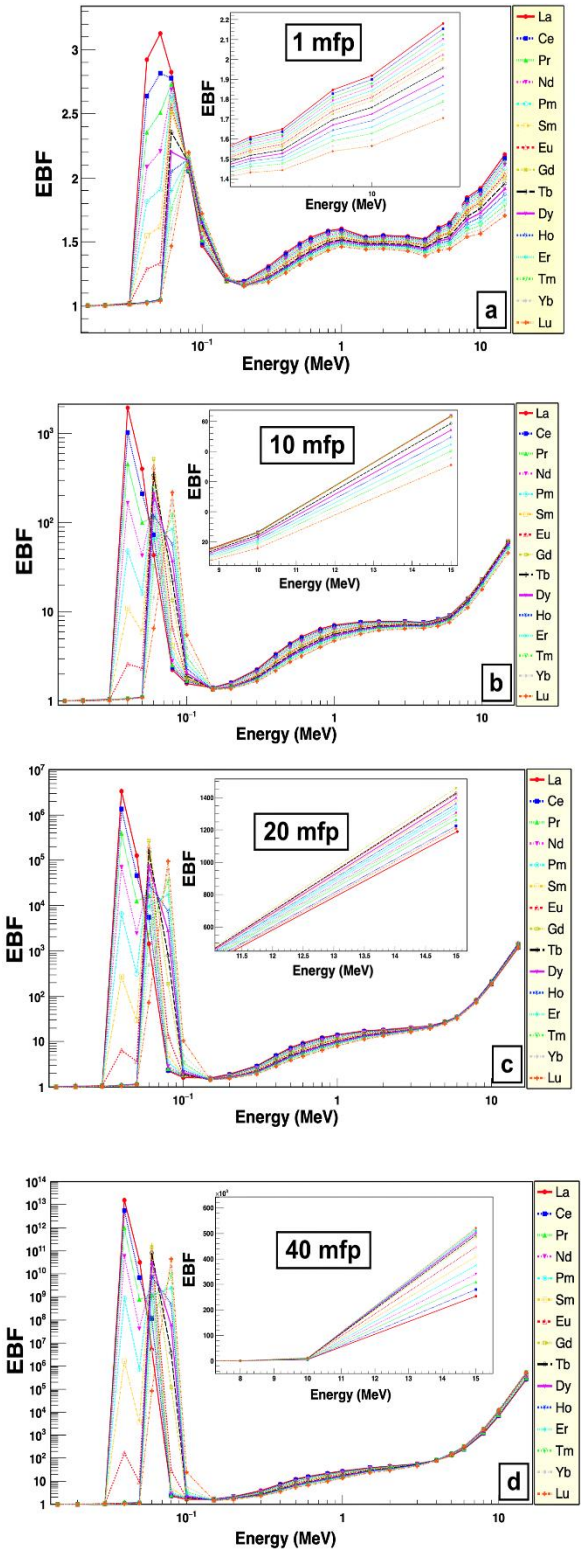

Figure 5. Variation of EBF with photon energy in the range of 0.015 to 15 MeV for Lanthanide group elements at various penetration depths for **(a)**1 mfp, **(b)** 10 mfp, **(c)** 20 mfp, **(d)** 40 mfp.

The Linear Attenuation Coefficient (LAC) values for each lanthanide element within the energy range of 200–2000 keV were compared with the results obtained from EpiXS and GATE simulations. These are presented in Table 2. The percentage difference was calculated using Eq. (8) and was found to be less than 5%.

According to Pyngrope's work, Erbium has the highest mass attenuation coefficient (0.03907 cm/g), while Lanthanum has the lowest (0.03646 cm/g), both measured with 4 MeV gamma radiation [35]. Erbium also has the lowest HVL (1.956 cm) and MFP (2.823 cm), making it the most effective lanthanide for radiation shielding at this energy level [35]. In our study, the results are consistent with the literature; based on the GATE simulation, the mass attenuation coefficient (MAC) of Erbium was found to be 0.039107 cm/g, while Lanthanum's MAC value was 0.036405 cm/g. Furthermore, according to both the GATE simulation and EpiX calculation, which show good agreement, the lowest HVL and MFP values are observed for Lutetium, with an HVL of 1.7707 cm and an MFP of 2.5545 cm. The highest values are found for Europium, with an HVL of 3.3924 cm and an MFP of 4.8943 cm.

4. Conclusion and Suggestions

The findings of this study underscore the varying radiation shielding capabilities of Lanthanide elements, with key parameters such as the MAC, LAC, HVL, and MFP. The observed decrease in MAC and LAC values with increasing photon energy underscores the transition from photoelectric interactions at lower energies to the predominance of Compton scattering and pair production at higher energies. The distinct peaks in attenuation values, correlated with the atomic structure of the elements, illustrate how atomic number influences shielding effectiveness, with Lutetium demonstrating superior performance due to its lowest HVL and MFP values. Conversely, Europium exhibited less effective shielding capabilities. Furthermore, the analysis of the EABF and EBF reveals critical insights into photon interactions, particularly the impact of energy range on these factors. Overall, this research provides valuable data that can inform the selection and optimization of Lanthanide materials for radiation shielding applications, paving the way for enhanced safety and efficiency in the nuclear and medical fields. Additionally, it establishes a foundation for investigating how the incorporation of rare earth elements into glass structures may alter their properties. Future studies should focus on exploring the practical applications of these findings in real-world settings, further advancing our understanding of radiation protection materials.

Table 2. Comparison of LAC Values for Lanthanide Elements: EpiXS vs. GATE Simulations.

Elements		Photon Energy (keV)				
		200	500	1000	1500	2000
		LAC (cm^{-1})				
Lanthanum (La)	**GATE**	2.5501	0.6311	0.3515	0.2864	0.2453
	EpiXS	2.6194	0.6238	0.3605	0.2848	0.2530
Cerium (Ce)	**GATE**	2.8613	0.6666	0.3928	0.3165	0.2743
	EpiXS	2.9784	0.6929	0.3963	0.3125	0.2776
Praseodymium (Pr)	**GATE**	3.0364	0.7100	0.4075	0.3353	0.2868
	EpiXS	3.1875	0.7250	0.4101	0.3227	0.2868
Neodymium (Nd)	**GATE**	3.2844	0.7574	0.4323	0.3378	0.3051
	EpiXS	3.4094	0.7586	0.4246	0.3334	0.2963
Promethium (Pm)	**GATE**	3.6717	0.7845	0.4314	0.3552	0.3150
	EpiXS	3.7147	0.8087	0.4480	0.3509	0.3119
Samarium (Sm)	**GATE**	3.8053	0.8212	0.4467	0.3465	0.3293
	EpiXS	3.9214	0.8361	0.4581	0.3580	0.3182
Europium (Eu)	**GATE**	2.7552	0.5754	0.3294	0.2404	0.2183
	EpiXS	2.8555	0.5959	0.3233	0.2521	0.2241
Gadolinium (Gd)	**GATE**	4.2475	0.8865	0.4586	0.3909	0.3291
	EpiXS	4.3897	0.9000	0.4821	0.3750	0.3333
Terbium (Tb)	**GATE**	4.6163	0.9108	0.4922	0.4021	0.3486
	EpiXS	4.7724	0.9587	0.5085	0.3946	0.3507
Dysprosium (Dy)	**GATE**	4.9806	0.9729	0.5124	0.4072	0.3493
	EpiXS	5.1120	1.0096	0.5288	0.4094	0.3638
Holmium (Ho)	**GATE**	5.2767	1.0191	0.5310	0.4063	0.3852
	EpiXS	5.4583	1.0599	0.5488	0.4238	0.3765
Erbium (Er)	**GATE**	5.7529	1.0885	0.5462	0.4268	0.3787
	EpiXS	5.8416	1.1146	0.5711	0.4397	0.3907
Thulium (Tm)	**GATE**	6.1296	1.1461	0.5856	0.4422	0.4031
	EpiXS	6.2485	1.1746	0.5951	0.4566	0.4056
Ytterbium (Yb)	**GATE**	4.6430	0.8474	0.4278	0.3301	0.2938
	EpiXS	4.7464	0.8774	0.4402	0.3369	0.2991
Lutetium (Lu)	**GATE**	6.9433	1.2390	0.6108	0.4613	0.4308
	EpiXS	7.0377	1.2836	0.6356	0.4850	0.4305

Statement of Research and Publication Ethics

The study is complied with research and publication ethics.

References

[1] F. Wall, "Rare earth elements," in *Encyclopedia of Geology*, 2nd ed., D. Alderton and S. Elias, Eds., Elsevier, pp. 680–693, 2021. [Online]. https://doi.org/10.1016/B978-0-08-102908-4.00101-6.

[2] J. A. Giacalone, "The market for the 'not-so-rare' rare earth elements," *J. Int. Energy Policy*, vol. 1, no. 1, pp. 11–18, 2012. [Online]. Available: https://doi.org/10.19030/jiep.v1i1.7013.

[3] S. B. Castor and J. B. Hedrick, "Rare earth elements," in *Materials Science and Chemistry*, G. E. Totten, Ed., CRC Press, 2006. [Online]. Available: https://doi.org/10.1002/0470862106.id683.

[4] P. F. Lou, X. B. Teng, Q. X. Jia, Y. Q. Wang, and L. Q. Zhang, "Preparation and structure of rare earth/thermoplastic polyurethane fiber for X-ray shielding," *J. Appl. Polym. Sci.*, vol. 136, no. 17, p. 47435, 2018.

[5] T. Cui, S. Duan, R. Chen, R. Wang, and Q. Jia, "Monte Carlo simulation study of rare earth/polypropylene composite shielding 120 KV medical X-ray," *J. Phys.: Conf. Ser.*, vol. 2539, no. 1, p. 012070, Jul. 2023.

[6] Y. Liu, X. Li, Y. Yin, Z. Li, H. Yao, Z. Li, and H. Li, "Design and computational validation of γ-ray shielding effectiveness in heavy metal/rare earth oxide–natural rubber composites," *Polymers*, vol. 16, no. 15, p. 2130, 2024.

[7] F.-H. Mai, Q.-P. Zhang, R. Wang, L.-C. Meng, Y. Zhang, J.-L. Li, P.-Q. Liu, Y.-T. Li, and Y.-L. Zhou, "Polymer fibers highly filled with styrene maleic anhydride-modified PbWO4 for improved wear comfort of γ-ray-shielding articles," *ACS Appl. Polym. Mater.*, vol. 4, pp. 6394–6402, 2022.

[8] M. Şahiner, Y. Z. Akgök, M. Arslan, and M. H. Ergin, "Dünyada ve Türkiye'de nadir toprak elementleri (NTE)," *Maden Tetkik ve Arama Genel Müdürlüğü*, Fizibilite Etütleri Daire Başkanlığı, 2017.

[9] Y. S. Rammah, A. A. Ali, R. El-Mallawany, and F. I. El-Agawany, "Fabrication, physical, optical characteristics and gamma-ray competence of novel bismuth-borate glasses doped with Yb_2O_3 rare earth," *Physica B: Condens. Matter*, vol. 583, p. 412055, 2020.

[10] Y. S. Rammah, F. I. El-Agawany, K. A. Mahmoud, R. El-Mallawany, E. Ilik, and G. Kilic, "FTIR, UV–Vis–NIR spectroscopy, and gamma rays shielding competence of novel ZnO-doped vanadium borophosphate glasses," *J. Mater. Sci.: Mater. Electron.*, vol. 31, no. 12, pp. 9099–9113, 2020.

[11] H. Jing, L. Geng, S. Qiu, H. Zou, M. Liang, and D. Deng, "Research progress of rare earth composite shielding materials," *J. Rare Earths*, vol. 41, no. 1, pp. 32–41, 2023.

[12] P. Fernandez-Arias, D. Vergara, and J. A. Orosa, "A global review of PWR nuclear power plants," *Appl. Sci.*, vol. 10, no. 13, p. 4434, 2020.

[13] P. Wu, M. Liu, J. G. Deng, J. J. Fu, Z. H. Deng, and Y. Q. Song, "Research progress of neutron shielding material," *Nucl. Chem. Mater.*, vol. 45, no. 9, pp. 4–8, 2017.

[14] A. A. Suresh, P. Vinothkumar, M. Mohapatra, M. Dhavamurthy, and P. Murugasen, "The effect of rare earth on the radiation shielding properties of transparent lead-free alumino-borophosphate glass system," *Radiat. Phys. Chem.*, vol. 193, p. 109941, 2022.

[15] E. S. A. Waly, G. S. Al-Qous, and M. A. Bourham, "Shielding properties of glasses with different heavy elements additives for radiation shielding in the energy range 15–300 keV," *Radiat. Phys. Chem.*, vol. 150, pp. 120–124, 2018.

[16] G. Lakshminarayana et al., "Investigation of structural, thermal properties and shielding parameters for multicomponent borate glasses for gamma and neutron radiation shielding applications," *J. Non-Cryst. Solids*, vol. 471, pp. 222–237, May 2017.

[17] R. Florez, A. Loaiza, C. H. C. Giraldo, and H. A. Colorado, "Calcium silicate phosphate cement with samarium oxide additions for neutron shielding applications in the nuclear industry," *Prog. Nucl. Energy*, vol. 133, p. 103650, 2021.

[18] M. Ma, M. E. Thomas, P. McGuiggan, and J. B. Spicer, "Weak absorption and scattering losses from the visible to the near-infrared in single-crystal sapphire materials," *Opt. Eng.*, vol. 59, no. 8, p. 87101, 2020.

[19] K. M. Mahmoud and Y. S. Rammah, "Investigation of gamma-ray shielding capability of glasses doped with Y, Gd, Nd, Pr, and Dy rare earth using MCNP-5 code," *Physica B: Condens. Matter*, vol. 577, p. 411756, 2020.

[20] P. Kaur, D. Singh, and T. Singh, "Gamma rays shielding and sensing application of some rare earth doped lead-alumino-phosphate glasses," *Radiat. Phys. Chem.*, vol. 144, pp. 336–342, 2018.

[21] W. F. Yang, Y. Liu, L. Yang, D. Li, and J. Li, "Research progress in shielding materials for nuclear radiation," *Mater. Rev.*, vol. 21, no. 5, pp. 82–87, 2007.

[22] B. Gan, S. C. Liu, Z. He, F. C. Chen, H. X. Niu, J. C. Cheng et al., "Research progress of metal-based shielding materials for neutron and gamma rays," *Acta Metall. Sin.*, vol. 7, pp. 68–75, 2021.

[23] S. Zhao, Z. P. Huo, G. Q. Zhong, H. Zhang, and L. Q. Hu, "Research progress of neutron and gamma-ray composite shielding materials," *J. Funct. Mater.*, vol. 52, no. 3, pp. 3001–3010, 2021.

[24] G. Jagannath, A. G. Pramod, K. Keshavamurthy, B. N. Swetha, B. Bheemaiah, R. Eraiah, R. Rajaramakrishna, R. Ramesh, P. Prajwal, V. Hegde, S. C. Prashantha, and M. S. Alhuthali, "Nonlinear optical, optical limiting and radiation shielding features of Eu^{3+} activated borate glasses," *Optik*, vol. 232, p. 166563, 2021, doi: 10.1016/j.ijleo.2021.166563.

[25] O. I. Sallam, Y. S. Rammah, I. M. Nabil et al., "Enhanced optical and structural traits of irradiated lead borate glasses via Ce^{3+} and Dy^{3+} ions with studying radiation shielding performance," *Sci. Rep.*, vol. 14, p. 24478, 2024, doi: 10.1038/s41598-024-73892-w.

[26] F. C. Hila, A. Asuncion-Astronomo, C. A. M. Dingle, J. F. M. Jecong, A. M. V. Javier-Hila, M. B. Z. Gili, C. V. Balderas, G. E. P. Lopez, N. R. D. Guillermo, and A. V. Amorsolo Jr., "EpiXS: A Windows-based program for photon attenuation, dosimetry and shielding based on EPICS2017 (ENDF/B-VIII) and EPDL97 (ENDF/B-VI.8)," *Radiat. Phys. Chem.*, vol. 182, p. 109331, 2021.

[27] PubChem, "Periodic Table," *National Center for Biotechnology Information*, [Online]. Available: https://pubchem.ncbi.nlm.nih.gov/periodic-table/. [Accessed: Aug. 3, 2024].

[28] T. Şahmaran and N. Yavuzkanat, "Evaluation of gamma and neutron radiation shielding parameters of some glass materials by Monte Carlo and theoretical methods," *Radiat. Eff. Defects Solids*, vol. 179, no. 3–4, pp. 489–500, 2024.

[29] American National Standards Institute (ANSI), "Gamma-ray attenuation coefficient and buildup factors for engineering materials," *ANS/ANSI-6.4.3*, 1991.

[30] Y. Karabul, "Bazalt numunelerde EABF ve EBF parametrelerinin yeni bir metot ile tayini," M.S. thesis, İstanbul Univ., Inst. of Science, Istanbul, 2014, pp. 13–14.

[31] P. S. Singh, T. Singh, and P. Kaur, "Variation of energy absorption buildup factors with incident photon energy and penetration depth for some commonly used solvents," *Ann. Nucl. Energy*, vol. 35, pp. 1093–1097, 2008.

[32] S. Bilici, A. Bilici, and F. Külahcı, "Comparison photon exposure and energy absorption buildup factors of CR-39 and Trivex optical lenses," *Turk. J. Sci. Technol.*, vol. 17, no. 1, pp. 23–35, 2022.

[33] N. Yavuzkanat, "Fosfor-sandviç tipi dedektör sisteminin toplam gama verimi için modellenen Geant4 tabanlı GATE simülasyonu," *ALKÜ Fen Bilimleri Dergisi,* vol. 2, no. 3, pp. 150–162, 2020, doi: 10.46740/alku.804473.

[34] N. Nagaraj, H. C. Manjunatha, Y. S. Vidya, L. Seenappa, K. N. Sridhar, and P. S. Damodara Gupta, "Investigations on lanthanide polymers for radiation shielding purpose," *Radiat. Phys. Chem.*, vol. 199, p. 110310, 2022, doi: 10.1016/j.radphyschem.2022.110310.

[35] A. Pyngrope, Study of Radiation Shielding Properties of Lanthanides, *Solvent and Glass*, 2023, ch. 4, pp. 26–38. ISBN: 978-620-6-76775-6.